Increasing dynamic range of NES by using geometric nonlinear damping

Etienne Gourc, Pierre-Olivier Mattei, Renaud Cote, Matteo Capaldo

Increasing dynamic range of NES by using geometric nonlinear damping

Etienne Gourc, Pierre-Olivier Mattei, Renaud Cote, Matteo Capaldo

Abstract

The paper deal with the passive control of resonant systems using nonlinear energy sink (NES). The objective is to highlight the benefits of adding nonlinear geometrical damping in addition to the cubic stiffness nonlinearity. The behavior of the system is investigated theoretically by using the mixed harmonic balance multiple scales method. Based on the obtained slow flow equations, a design procedure that maximize the dynamic range of the NES is presented. Singularity theory is used to express conditions for the birth of detached resonance cure independently of the forcing frequency. It is shown that the presence of a detached resonance curve is not necessarily detrimental to the performance of the NES. Moreover, the detached resonce curve can be completely suppressed by adding nonlinear damping. The results of the design procedure are the compared to numerical simulations.

1 Introduction

Nonlinear energy sinks (NES) are strongly nonlinear oscillator that are used to mitigate vibration of a host system through targeted energy transfer. One of the main feature of NES, which is a consequence of their essential nonlinear nature is their ability to enter in resonance capture with the system to which their are attached, giving them a broadband capability [13]. When the primary system is subjected to harmonic excitation, the system exhibit relaxation oscillation denoted as strongly modulated response (SMR) which is also a typical feature of systems with NES [11]. One of the main drawback of NES when used to control an harmonically excited system is the possible presence of a high amplitude detached resonance curve. Specific design procedure have been developed to ensure a safe operating region of the system, at the price of limited performance of the NES [10, 4]. A promising way to overcome this difficulty is the introduction of nonlinear damping in addition to linear viscous damping. This has been first proposed in [12] where the authors considered piecewise-quadratic damping. It was shown that by imposing a fairly low damping at low amplitude and a higher damping at high amplitude can lead to a complete elimination of the detached resonance curve. In [1], the dynamics of a NES with geometrical damping is investigated under transient loading. They showed that the nonlinear damping can induce transient instability caused by a bifurcation to $1:3$ resonance capture. The behavior of a NES with global and local potential as well as nonlinear damping has been analyzed theoretically in [6]. Recently, the behavior of a NES with geometrical damping used to control a toy model of floating offshore wind turbine was investigated in [8]. They confirmed both theoretically and by using extensive numerical simulation that the addition of nonlinear damping can in certain condition completely suppress the detached resonance curve. Experimental investigation of nonlinear damping, not in the context of NES, is reported in [9], where a nonlinear damping element is realized geometrically at a beam tip.

The objective of the present paper is to investigate the benefits induced by the addition of geometrical nonlinear damping. Section 2 is devoted to the presentation of the studied system. Section 3 is devoted to the theoretical analysis of the system. First the equation of motions are analyzed by using the multiple scales-harmonic balance method (MSHBM) [7] allowing us to obtain the expression of the slow invariant manifold (SIM) and the slow flow modulation equation. In the same section, the folded singularity are expressed and interpreted as a grazing flow and condition for the existence of detached resonance curve is expressed by using singularity theory [3, 5]. The tuning procedure enabling to discriminate problematic and non problematic detached resonance curve is presented in section 4.

2 Description of the system

The system considered in the present paper is the same as in [1] and consists in a linear oscillator coupled to an embedded NES with geometrical nonlinear stiffness and damping. The equation of motion are given by

$$\begin{aligned} &M\ddot{x} + C\dot{x} + Kx + c\dot{w} + rw^3 + dw^2\dot{w} = A\cos(\Omega t) \\ &m(\ddot{x} - \ddot{w}) - c\dot{w} - rw^3 - dw^2\dot{w} = 0 \end{aligned} \tag{1}$$

where $x(t)$ and $w(t)$ are the displacement of the linear oscillator and the relative displacement of the NES, respectively. The dots denote differentiation with respect to time t. M, C, and K are the mass, damping and stiffness of the linear oscillator, respectively. c, r and d are the damping, cubic nonlinear stiffness and nonlinear damping of the NES, respectively. Adimensional parameters are introduced as follows

$$\begin{aligned} &\tilde{t} = \omega_1 t, \quad \omega_1 = \sqrt{\tfrac{K}{M}}, \quad \zeta = \tfrac{C}{2M\omega_1}, \quad \mu = \tfrac{c}{m\omega_1} \\ &\kappa = \tfrac{r}{m\omega_1^2}, \quad G = \tfrac{A}{M\omega_1^2}, \quad \omega = \tfrac{\Omega}{\omega_1}, \quad \lambda = \tfrac{d}{m\omega_1} \end{aligned} \tag{2}$$

Substituting into Eq. (1) yields to the following adimensional equation of motion

$$\begin{aligned} &\ddot{x} + 2\zeta\dot{x} + x + \epsilon(\mu\dot{w} + \kappa w^3 + \lambda w^2\dot{w}) = G\cos(\omega t) \\ &\epsilon(\ddot{x} - \ddot{w} - \mu\dot{w} - \kappa w^3 - \lambda w^2\dot{w}) = 0 \end{aligned} \tag{3}$$

where the tilde has been dropped for brevity and the dots now represent the derivative with respect to adimensional time. $\epsilon = m/M \ll 1$ is the mass ratio.

3 Nonlinear analysis

The behavior of the system is analyzed theoretically using the mixed multiple scales-harmonic balance method (MSHBM) [7]. Independent time scales $t_i = \epsilon^i t$ are introduced and the displacements are expanded as

$$\begin{aligned} &x(t;\epsilon) = x_0(t_0,t_1) + \epsilon x_1(t_0,t_1) + \dots \\ &w(t;\epsilon) = w_0(t_0,t_1) + \epsilon w_1(t_0,t_1) + \dots \end{aligned} \tag{4}$$

The damping of the primary system ζ as well as the forcing amplitude G are considered small and are scaled such that $\zeta = \epsilon\zeta$ and $G = \epsilon G$. Substituting Eq. (4) into Eq. (3) and collecting terms of same power of ϵ gives

$$\mathcal{O}(\epsilon^0): \quad d_0^2 x_0 + x_0 = 0 \tag{5}$$

$$\begin{aligned} \mathcal{O}(\epsilon^1): \quad & d_0^2 x_1 + x_1 = -2d_0d_1x_0 - 2\zeta d_0 x_0 - \mu d_0 w_0 - \kappa w_0^3 - \lambda w_0^2 d_0 w_0 + G\cos(\omega t_0) \\ & d_0^2(w_0 - x_0) + \mu d_0 w_0 + \kappa w_0^3 + \lambda w_0^2 d_0 w_0 = 0 \end{aligned} \tag{6}$$

The solution at order ϵ^0 is expressed by

$$x_0(t_0,t_1) = \frac{1}{2}X(t_1)\mathrm{e}^{it_0} + \text{c.c.} \tag{7}$$

Now we deal with the equations at order ϵ^1. Since the second equation does not admit a closed form solution, according to the MSHBM, we seek an approximate solution of the form

$$w_0(t_0,t_1) = \frac{1}{2}W(t_1)\mathrm{e}^{it_0} + \text{c.c.} \tag{8}$$

Substituting Eq. (7, 8) into the second equation of Eq.(6) and balancing terms corresponding to the first harmonic yields

$$X = (1 - i\mu)W - \frac{1}{4}(3\kappa + i\lambda)W^2W^* \tag{9}$$

Equation (9) represents the slow invariant manifold (SIM) of the problem. The behavior of the system is analyzed in the vicinity of the resonance of the primary system. Accordingly, a detuning parameter is introduced as $\omega = 1 + \epsilon\sigma$. Substituting Eq. (7, 8) into the first equation of Eq.(6) and eliminating secular terms reads

$$d_1 X = -\zeta X - \frac{1}{2}\mu W + \frac{1}{8}(3i\kappa - \lambda)W^2 W^* - \frac{1}{2}iG\mathrm{e}^{i\sigma t_1} \tag{10}$$

Going back to true time t and reabsorbing ϵ the modulation equation is obtained as

$$\dot{X} = -\zeta X - \epsilon\left(\frac{1}{2}\mu W + \frac{1}{8}(3i\kappa - \lambda)W^2 W^*\right) - \frac{1}{2}iG\mathrm{e}^{i\sigma t} \tag{11}$$

Since we are interested in the dynamic of the system under $1:1$ resonance capture, i.e. on the SIM, Eq. (9) is substituted into Eq. (11). Expressing $W(t) = b(t)\mathrm{e}^{i\beta(t)}$ and splitting into real and imaginary parts gives

$$\begin{array}{l} \dot{b} = \frac{f_1(b,\theta)}{g(b)} \\ \dot{\theta} = \frac{f_2(b,\theta,\sigma)}{g(b)} \end{array} \tag{12}$$

where the new phase variable $\theta(t) = \epsilon\sigma t - \beta$ has been introduced to transform the system into an autonomous one. Expressions of f_1 and f_2 are given in appendix. The fixed points of the system are computed by setting $f_1 = f_2 = 0$.

3.1 Analysis of the SIM

Substituting polar expression of $W(t)$ and $X(t) = a(t)\mathrm{e}^{i\alpha(t)}$ into Eq. (9), the real valued expression of the SIM is obtained as

$$A = \frac{1}{16}\left[(3\kappa B - 4)^2 B + (\lambda B + 4\mu)^2 B\right] \tag{13}$$

where $A = a^2$ and $B = b^2$. The values of local extremums B_1 and B_2 are found by equating the derivative of the right hand side of Eq. (13) with respect to B to zero, giving

$$B_i = \frac{4}{3}\frac{6\kappa - 2\mu\lambda \mp \sqrt{h}}{9\kappa^2 + \lambda^2} \tag{14}$$

with

$$h = -27\kappa^2\mu^2 + \lambda^2\mu^2 - 24\kappa\lambda\mu + 9\kappa^2 - 3\lambda^2 \tag{15}$$

Note that the SIM admits extremums only if $h > 0$. It is well known that this topology of SIM can give rise to strongly modulated response. An example of SIM for $\mu = 0.1$, $\kappa = 1$ and $\lambda = 0.1$ is depicted in Fig. 3.1.

3.2 Folded singularities

In addition to classical fixed points of the slow flow system, computed by setting $f_1 = f_2 = 0$ and $g \neq 0$, it is well known that systems with NES also admit singular fixed points denoted as folded singularities [11]. The folded singularities are found by setting $f_1 = f_2 = g = 0$. Physically speaking, folded singularity allow the flow to jump from the lower to the upper branch of the SIM. On the phase plane (θ, b), the transition from a situation where the slow flow remains on the lower part of the SIM to a situation where the flow can jumps to the higher branch of the SIM corresponds to a grazing flow at $b = b_1$, that is

$$\left.\frac{db}{d\theta}\right|_{b=b_1} = 0 \tag{16}$$

with

$$\frac{db}{d\theta} = \frac{\frac{db}{dt}}{\frac{d\theta}{dt}} = \frac{f_1}{f_2} \tag{17}$$

Such that the grazing condition simply reads $f_1(b_1, \theta) = 0$. From this relation, it is possible to express the minimal amplitude G_{fs_1} that give rise to the existence of folded singularities. Note that since f_1 is independent of σ, G_{fs_1} is valid for the whole excitation frequency range. An example of grazing bifurcation yielding to the birth of a pair of folded singularities is depicted in Fig. 3.2.

For completeness, folded singularity on the upper branch of the SIM at $b = b_2$ can be expressed similarly, i.e. $f_1(b_2, \theta) = 0$, and the critical forcing amplitude yielding to their appearance is denoted by G_{fs_2}.

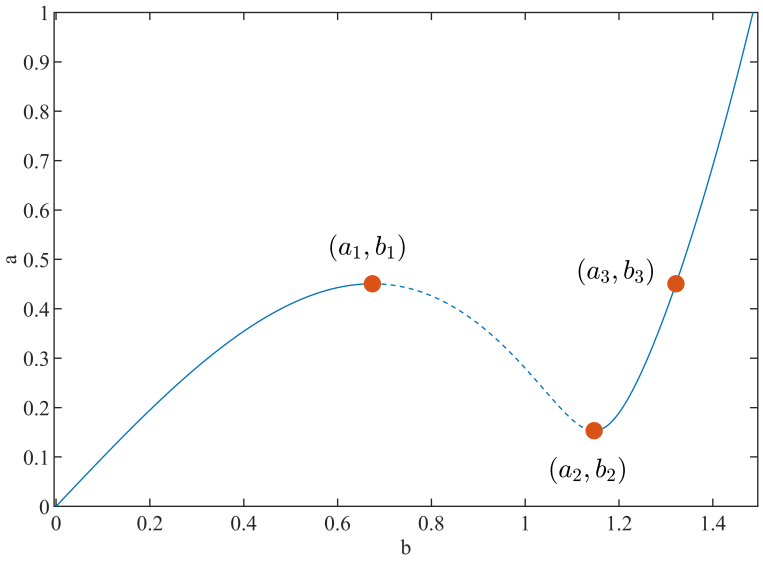

Figure 1: SIM for $\mu = 0.1$, $\kappa = 1$ and $\lambda = 0.1$. Solif and dashed lines correspond to stable and unstable branches, respectively.

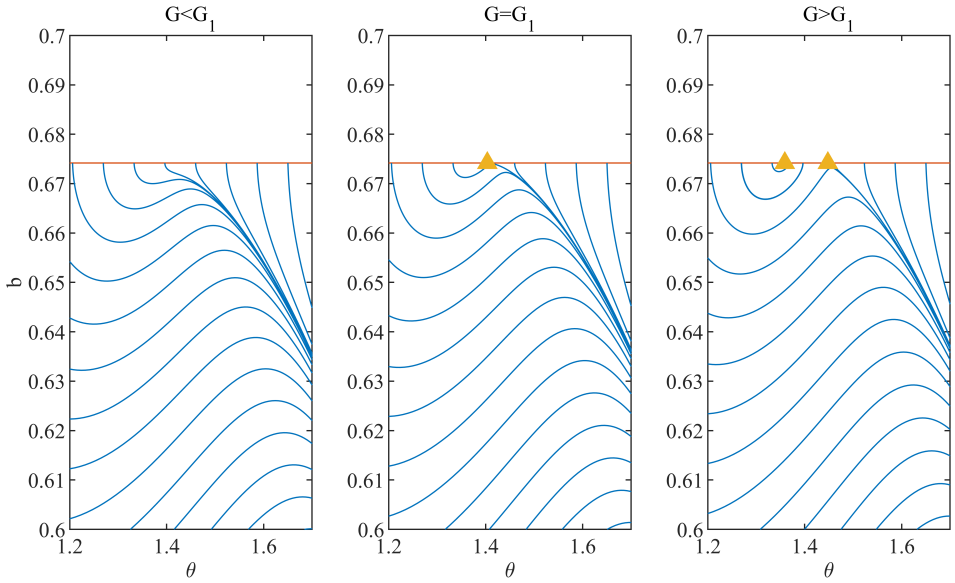

Figure 2: Phase plot for $\mu = 0.1$, $\epsilon = 0.01$, $\zeta = 0.01$, $\kappa = 1$, $\lambda = 0.1$ and $\sigma = 1$ for three value of G around $G_1 = 0.0101$. Solid reg line corresponds to $b = b_1$ and orange triangle to the folded singularities.

3.3 Detached resonance curve

As mentioned earlier, systems with NES can exhibit a detached resonance curve that can yield to high amplitude oscillations and therefore deteriorate the performance of the NES. A polynomial expression for the amplitude of the fixed points b can be obtained by solving $f_1 = f_2 = 0$ for the trigonometric terms and using trigonometric identity. The fixed points b are now found by solving

$$f_3(b, \sigma) = 0 \tag{18}$$

Singularity theory is a powerful tool to classify the different topologies of frequency response curve [3]. Here, we are particularly interested in isola and simple bifurcation singularities that are responsible for the creation of the isola or to the merging of the detached resonance curve with the main frequency response curve, respectively. The defining conditions for these singularities are given by

$$\begin{array}{lllllll} \text{isola :} & f_3 = 0, & \frac{\partial f_3}{\partial b} = 0, & \frac{\partial f_3}{\partial \sigma} = 0, & \frac{\partial^2 f_3}{\partial b^2} \neq 0, & \det(d^2 f_3) > 0 \\ \text{simple bifurcation :} & f_3 = 0, & \frac{\partial f_3}{\partial b} = 0, & \frac{\partial f_3}{\partial \sigma} = 0, & \frac{\partial^2 f_3}{\partial b^2} \neq 0, & \det(d^2 f_3) < 0 \end{array} \tag{19}$$

where $d^2 f_3$ is the Hessian matrix of $f_3(b, \sigma)$. Closed form solutions are not available, however, Eq. (19) can be combined to express a sixth order polynomial in b^2 that can be efficiently solved using any root finding algorithm and the corresponding forcing amplitude can be retrieved by using the fixed point equation. Remarkably, the obtained result is independent of σ. The critical forcing amplitudes corresponding to isola and simple bifurcation singularities are denoted G_{drc} and G_{sb}, respectively. Note however that the presence of a detached resonance curve does not necessarily yields to higher amplitude compared to the principal resonance curve. An example is depicted in Fig. 3.3 for two different set of parameters.

Clearly, in the upper case, the detached resonance curve is problematic as it yield to high amplitude oscillation. Problematic cases can be easily detected by looking at the amplitude b at which the detached resonance curve is created. Exploiting the topology of the SIM, if the isola singularity is located at $b > b_3$ it will cause high amplitude oscillations of the primary system, as shown in Fig. 3.3.

4 NES sizing

In this section, the sizing of the NES is addressed and can be formulated as follows: *Given a maximal allowed amplitude of the primary system, what are the parameters of the NES that maximize the forcing amplitude?*

It is known that the the control mechanism of NES under harmonic forcing involves strongly modulated response (SMR) regimes. This regime corresponds to relaxation oscillation where the dynamics successively jumps between the two stable branches of the SIM. If no other attractors (i.e. fixed points) are present, the maximal amplitude of the primary system is directly governed by the shape of the SIM and corresponds to the point labeled a_1 in Fig. 3.1. The first step of the design procedure consists in determining the nonlinear stiffness coefficient κ to fix the maximal amplitude a_1. This is done by using the expression of the SIM Eq. (13) at $b = b_1$. Notice that the obtained expression is invariant with respect to a_1 if $\kappa = \tilde{\kappa}/a_1^2$ and $\lambda = \tilde{\lambda}/a_1^2$ such that without loss of generality we choose $a_1 = 1$. The value of κ as a function of the linear and nonlinear damping μ and λ allows to reduce the design space by one and is depicted in Fig. 4.

The second step consists in identifying the parameter space where $a \leq a_1$. Exploiting the shape of the SIM, an equivalent condition in terms of the relative amplitude of the NES reads $b \leq b_3$. A necessary but not sufficient condition to express the maximal forcing amplitude $G_{\max}$ such that $b \leq b_3$ is given by

$$\left.\frac{\partial b}{\partial \sigma}\right|_{b=b_3} = 0 \tag{20}$$

Using implicit differenciation, condition in Eq. (20) becomes

$$f_3 = 0, \quad \left.\frac{\partial f_3}{\partial \sigma}\right|_{b=b_3} = 0 \tag{21}$$

As mentioned, this condition is however not sufficient to guaranty that $a \leq a_1$ due to the possible presence of a detached resonance curve at higher amplitude. As explained in the previous section, problematic detached resonance curves are easily identified by looking at the amplitude

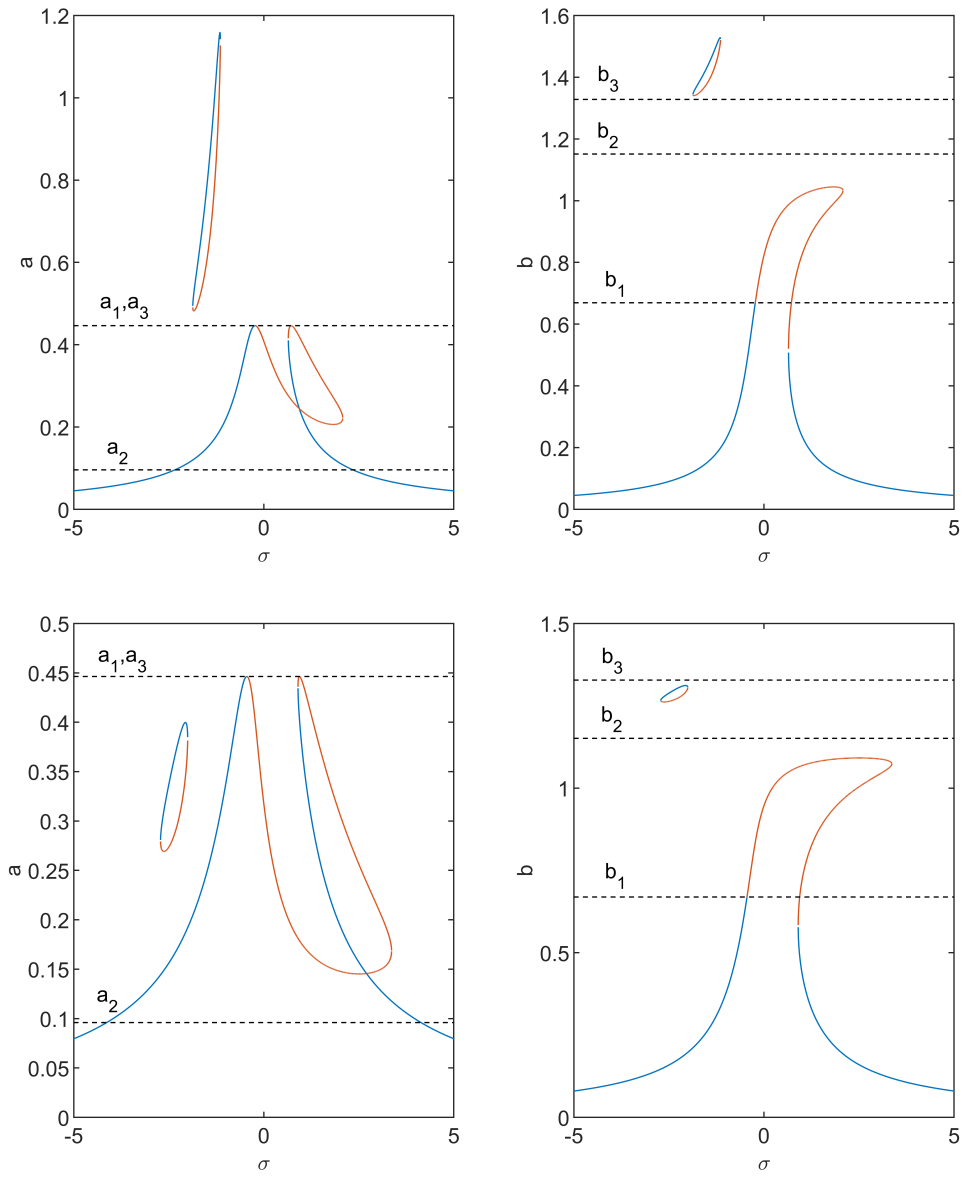

Figure 3: Frequency response curve for $\epsilon = 0.01$, $\lambda = 0.1$, $\kappa = 1$, $\mu = 0.05$. Up : $\zeta = 0.001$, $G = 0.0045$, down : $\zeta = 0.005$, $G = 0.08$. Blue and orange lines corresponds to stable and unstable solution, respectively. Dashed lines indicates the singular points of the SIM.

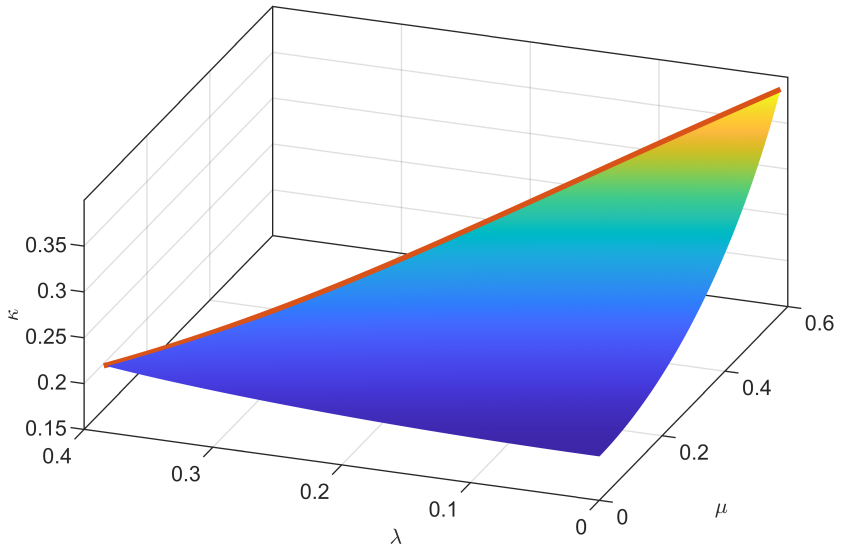

Figure 4: Evolution of κ as a function of μ and λ for $a_1 = 1$. Red line corresponds to the limit where the SIM admit a double root.

b corresponding to the isola singularity. If $b > b_3$, the resulting isola will result to amplitude of oscillation greater than a_1. On the contrary, if a detached resonance curve is created in the lower portion of the SIM ($b < b_3$), while the growth of this detached resonance curve until $a = a_1$ will be captured by Eq. (21).

Examples of obtained sizing diagram are depicted in Fig. 4. In both cases $\epsilon = 0.01$ and $\mu = 0.1$. On the left diagram $\zeta = 0.001$ while on the righ diagram $\zeta = 0.01$. Solid and dashed blue lines corresponds to folded singularities occuring on $b = b_1$ and $b = b_2$, respectively. Solid green lines corresponds to the maximal forcing amplitude $G_{\max}$. Orange and yellow lines correspond to problematic and non-problematic isola singularity, respectively and finally purple dash-dotted lines corresponds to simple bifurcation singularity yielding to the merging of the detached resonance curve with the main resonance curve. The safe region of operation of the NES is indicated by the grey area.

Frequency response curves corresponding to different area of the sizing diagram are depicted in Fig. 4. Bellow the first folded singularity (Fig. 4(a)), SMR regime is not possible and the NES behaves in a quasi-linear manner. In the zone corresponding to Fig. 4(b), i.e. between both folded singularities and bellow any detached resonance curve, the periodic solutions around $\sigma = 0$ are unstable and the only possible response is SMR. When the forcing amplitude is increased above the second folded singularity and bellow the maximal forcing amplitude (Fig. 4(c,h)), SMR regime can be replaced by stable periodic response, but still satisfying the design criteria (i.e. $a < 1$). Fig. 4(d,f) illustrates again problematic and non problematic detached resonance curve, similarly to Fig. 3.3. In the case depicted in Fig. 4(f), the presence of the detached resonance curve does not restrict the design area. In the case presented in Fig. 4(g), the forcing amplitude is increased above the simple bifurcation singularity corresponding to the merging of the detached resonance curve. In this case, the design criteria is still satisfied. In the case depicted in Fig. 4(e,i), the parameters of the system are above the maximal forcing amplitude $G_{\max}$, and even if no detached resonance curve are present, the stable periodic solution exceed the maximal amplitude (i.e. $a > 1$). Nevertheless, for both sizing diagram, it can be noticed that the addition of nonlinear damping significantly increase the dynamic range of the NES.

The proposed sizing procedure is compared to numerical simulation in Fig. 4 where the maximal amplitude of the primary oscillator obtained from numerical integration is depicted for various excitation amplitude and frequency for $\epsilon = 0.01$, $\zeta = 0.01$, $\mu = 0.1$, $\lambda = 0.16$, and $\kappa = 0.214$. The red plane and dashed lines correspond to the maximal allowed amplitude. The first vertical dashed line corresponds to the critical forcing yielding to the birth of a pair of folded singularity $G_{\text{fs}_1} = 0.0244$ while the second vertical dashed line corresponds to the maximal forcing amplitude $G_{\max} = 0.0453$. The location of the control plateau for $G \in [G_{\text{fs}_1}, G_{\max}]$ is in very good agreement with numerical simulations while the maximal amplitude is underestimated by the theoretical

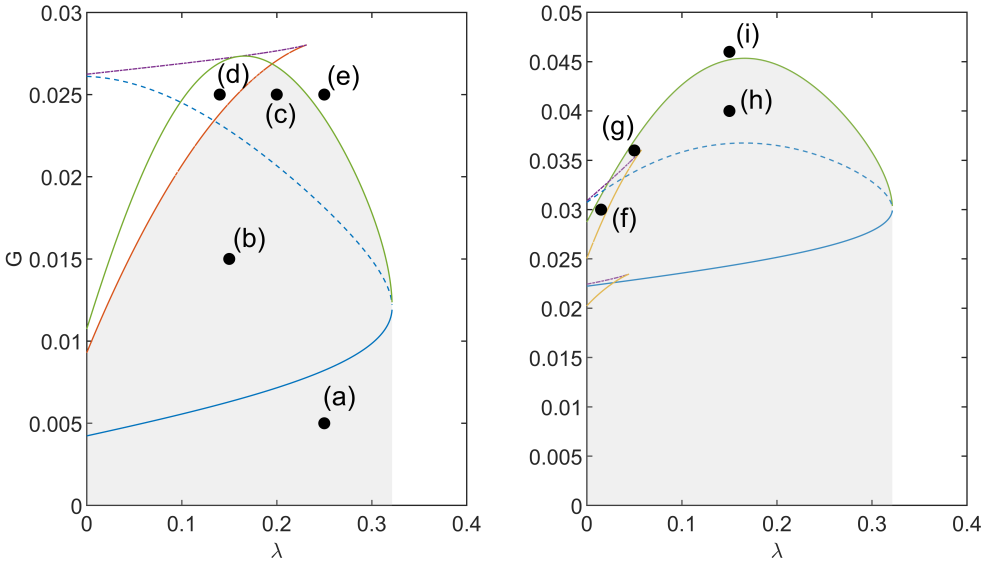

Figure 5: Evolution of κ as a function of μ and λ for $a_1 = 1$. Red line corresponds to the limit where the SIM admit a double root.

analysis.

As illustrated in Fig. 4 where $G = 0.04$ and $\sigma = 1.1$, this is due to the fact that the jump between the branch of the SIM does not occur as a discontinuous phase trajectory when $\epsilon \neq 0$. Note that this fact has been investigated theoretically in [2] by interpreting the jump as a dynamic fold bifurcation.

5 Conclusion

The objective of the present paper was to investigate the potential benefits of geometric nonlinear damping on NES. To this end, the dynamics of the system has been analyzed by using the mixed multiple scales - harmonic balance method. A simple design procedure is presented and can be simply summarized as follow: *given a maximal allowable amplitude of the primary system, what are the parameters of the NES that maximize the forcing range.* The main theoretical findings presented throughout the design procedure are twofold:

- Exploiting the topology of the SIM, in combination with singularity theory, we are able to distinguish parameters that yield to unacceptable or acceptable detached resonance curves.
- Again exploiting the topology of the SIM and the expression of the fixed points allow us to express a maximal forcing amplitude independently of the forcing frequency yielding to a given amplitude of the host oscillator.

The conjunction of these two criteria allow us to define a safe design space of the NES guaranteeing that the vibration amplitude of the primary oscillator is bellow a certain threshold. Finally, this design procedure highlight the benefits of nonlinear damping with a significant increase of the maximal allowable forcing amplitude.

Appendix A

The expressions of f_1, f_2 and g given in Eq. (12) are given by

$$\begin{aligned} f_1(b,\theta) &= b\left(-\zeta\left(9\kappa^2+\lambda^2\right)b^5+2\left(12\kappa\zeta-\epsilon\lambda-4\lambda\mu\zeta\right)b^3-8\left(2\mu^2\zeta+\epsilon\mu+2\zeta\right)b\right. \\ &\quad \left.+8G\mu\cos\theta+2G\left(3\kappa b^2+4\right)\sin\theta\right) \\ f_2(b,\theta) &= 3\epsilon(9\kappa^2+\lambda^2)(2\sigma+1)b^5+4\left(\epsilon(8\lambda\mu\sigma-24\kappa\sigma+4\lambda\mu-3\kappa)+4\zeta(\lambda+3\kappa\mu)\right)b^3 \\ &\quad +16\epsilon\left(2\mu^2\sigma+\mu^2+2\sigma\right)b-4G(9\kappa b^2-4)\cos\theta-4G(3\lambda b^2+4\mu) \\ g(b) &= 2b\left(3(\lambda^2+9\kappa^2)b^4+16(\lambda\mu-3\kappa)b^2+16(\mu^2+1)\right) \end{aligned} \tag{22}$$

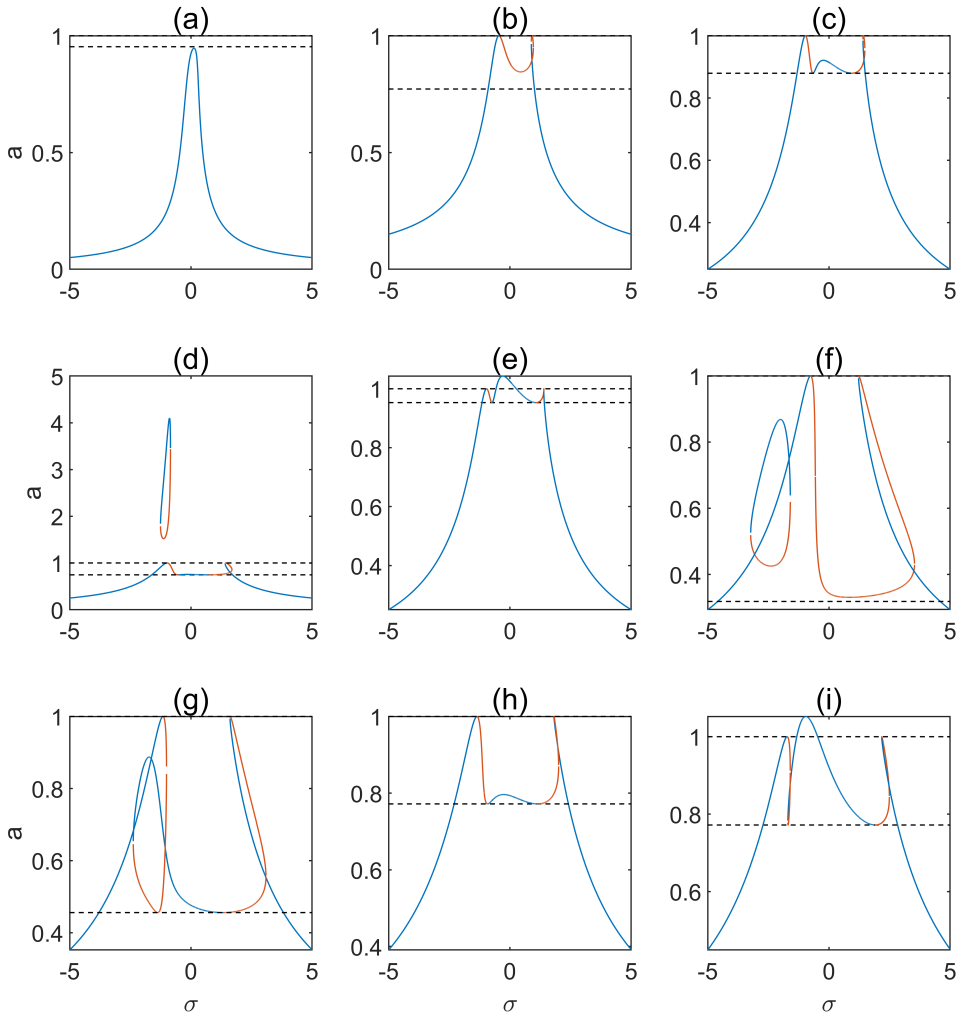

Figure 6: Frequency response curve of the primary oscillator corresponding to points in Fig. 4.

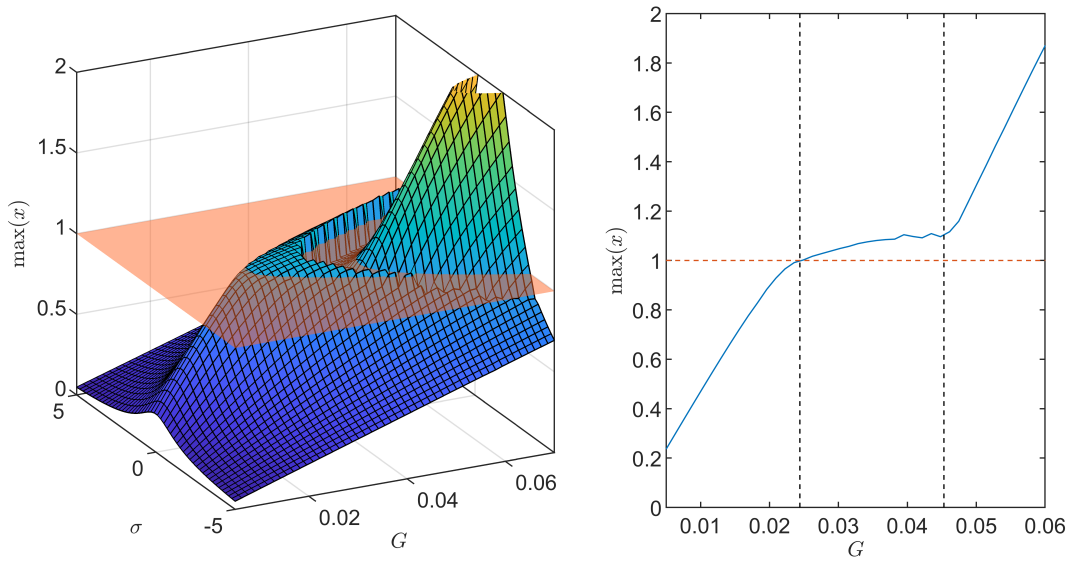

Figure 7: Amplitude of the primary oscillator as a function of the frequency detuning σ and forcing amplitude G for $\epsilon = 0.01$, $\zeta = 0.01$, $\mu = 0.1$, $\lambda = 0.16$, and $\kappa = 0.214$. Red plane (dashed line) corresponds to the theoretical maximal allowed amplitude and dashed vertical lines corresponds to G_{fs_1} (left) and $G_{\max}$ (right).

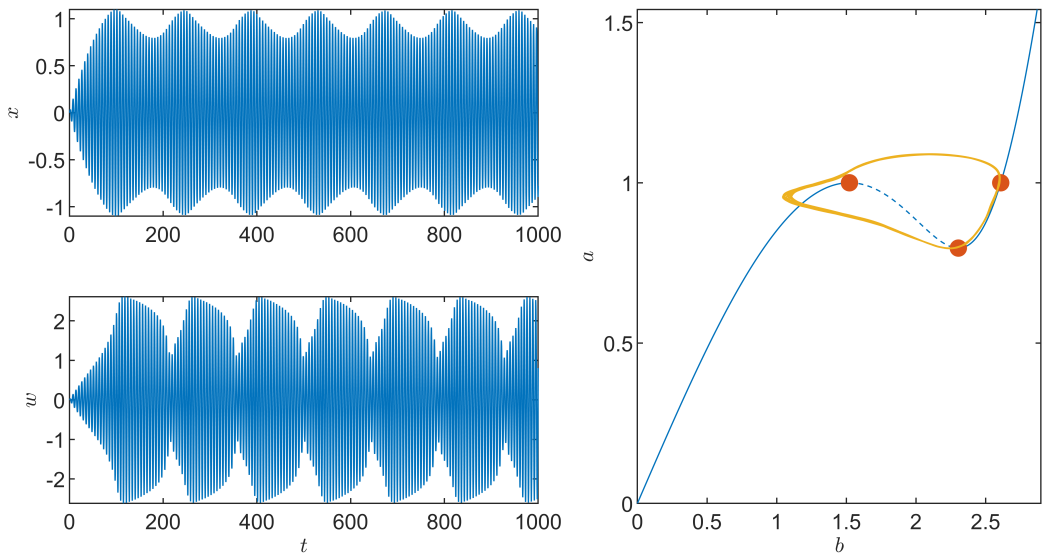

Figure 8: Example of strongly modulated response and projection on the SIM obtained for $\epsilon = 0.01$, $\zeta = 0.01$, $\mu = 0.1$, $\lambda = 0.16$, $\kappa = 0.214$, $\sigma = 1.1$ and $G = 0.04$.

References

[1] D. Andersen, Y. Starosvetsky, A. Vakakis, and L. Bergman. Dynamic instabilities in coupled oscillators induced by geometrically nonlinear damping. *Nonlinear Dynamics*, 67:807–827, 2012.

[2] B. Bergeot. Scaling law for the slow flow of an unstable mechanical system coupled to a nonlinear energy sink. *Journal of Sound and Vibration*, 503:116109, 2021.

[3] I. Cirillo, G. Habib, G. Kerschen, and R. Sepulchre. Analysis and design of nonlinear resonances via singularity theory. *Journal of Sound and Vibration*, 392:295–306, 2017.

[4] E. Gourc, G. Michon, S. Seguy, and A. Berlioz. Experimental investigation and design optimization of targeted energy transfer under periodic forcing. *Journal of Vibration and Acoustics*, 136(2), 2014.

[5] G. Habib, I. Cirillo, and G. Kerschen. Isolated resonances and nonlinear damping. *Nonlinear Dynamics*, 93:979–994, 2018.

[6] Y. Liu, G. Chen, and X. Tan. Dynamic analysis of the nonlinear energy sink with local and global potentials: geometrically nonlinear damping. *Nonlinear Dynamics*, 101:2157–2180, 2020.

[7] A. Luongo and D. Zulli. Dynamic analysis of externally excited nes-controlled systems via a mixed multiple scale/harmonic balance algorithm. *Nonlinear Dynamics*, 70:2049–2061, 2012.

[8] P-0. Mattei and R. Côte. Optimization of a dynamic absorber with nonlinear stiffness and damping for the vibration control of a floating offshore wind turbine toy model. *Journal of Theoretical, Computational and Applied Mechanics*, 2023.

[9] A. Mojahed, K. Moore, L. Bergman, and A. Vakakis. Strong geometric softening–hardening nonlinearities in an oscillator composed of linear stiffness and damping elements. *International Journal of Non-Linear Mechanics*, 107:94–111, 2018.

[10] Y. Starosvetsky and O. Gendelman. Response regimes of linear oscillator coupled to nonlinear energy sink with harmonic forcing and frequency detuning. *Journal of Sound and Vibration*, 315(3):746–765, 2008.

[11] Y. Starosvetsky and O. Gendelman. Strongly modulated response in forced 2dof oscillatory system with essential mass and potential asymmetry. *Physica D: Nonlinear Phenomena*, 237(13):1719–1733, 2008.

[12] Y. Starosvetsky and O. Gendelman. Vibration absorption in systems with a nonlinear energy sink: nonlinear damping. *Journal of Sound and Vibration*, 324(3-5):916–939, 2009.

[13] A. Vakakis and O. Gendelman. Energy pumping in nonlinear mechanical oscillators: part ii—resonance capture. *J. Appl. Mech.*, 68(1):42–48, 2001.